Research Article

Nano Biomed Eng

Green Synthesis of Zinc Oxide Nanoparticles Using *Pistacia lentiscus* L. Leaf Extact and Evaluating their Antioxydant and Antibacterial Properties

Rihab Haddi[1], Aicha Maria El Kharraz[2], Mimouna Ikram Kerroumi[2]

[1] Laboratory of Valorization of Vegetal Resource and Food Security in Semi-arid Areas in southwest Algeria, Department of Biology, Faculty of Sciences, TAHRI Mohamed university Bechar, Algeria

[2] Department of Biology, Faculty of Sciences, TAHRI Mohamed University Bechar, Algeria

Received: Sep. 13, 2023; **Revised:** Oct. 15, 2023; **Accepted:** Nov. 13, 2023

Citation: R. Haddi, A.M. El Kharraz, M.I. Kerroumi. Green synthesis of zinc oxide nanoparticles using *pistacia lentiscus* L. leaf extact and evaluating their antioxydant and antibacterial properties. *Nano Biomedicine and Engineering*, 2024, 16(2): 232−247.

http://doi.org/10.26599/NBE.2024.9290056

Abstract

Pistacia lentiscus leaf extract has been used as a reducing and capping agent for the green production of zinc oxide nanoparticles (ZnO NPs) to evaluate their antioxidant and antibacterial properties. The optical and structural properties were determined by ultraviolet–visible (UV–Vis) spectra, Fourier transform infrared spectroscopy (FTIR), and X-ray diffraction (XRD). In the UV–Vis spectra, an absorption peak at 310 nm was observed, whereas the FTIR spectra revealed a peak at 680 cm^{-1}, attributed to the vibration of ZnO NPs and confirmed their formation. X-ray analysis showed the crystalline quality of the ZnO product, with well-defined peaks on the (002), (100), and (101) planes, confirming a hexagonal structure (JCPDS-file: 36-1451). The grain size of the ZnO NPs was approximately 33.90 nm in diameter. Using scanning electron microscopy coupled with energy-dispersive X-ray spectroscopy (EDS), the morphology of the nanoparticles resembled dried cotton, whereas EDS confirmed the presence of zinc (Zn) and oxygen (O). The evaluation of antioxidant activity involved the DPPH test, thin-layer chromatography (TLC) bioautography, and spectrophotometric assay. The methanolic extract exhibited high antiradical potential, followed by aqueous, etheric, and finally ZnO NPs. Testing the antibacterial activity against two Gram-positive bacterial strains (*Staphylococcus aureus* and *Bacillus cereus*) and two Gram-negative strains (*Escherichia coli* and *Pseudomonas aeruginosa*) involved determining the minimum inhibitory concentration (MIC) and minimum bactericidal concentration (MBC). The results showed that zinc oxide nanoparticles displayed considerable antibacterial effects compared with crude extracts, demonstrating inhibition zones of (24 ± 1) mm and (20 ± 2) mm, respectively, against *E. coli* and *P. aeruginosa*, with a bactericidal effect evident by a MBC/MIC ratio of 2.

Keywords: phytochemical screening; zinc oxide nanopartices (ZnO NPs); green synthesis; *Pistacia lentiscus* L.; antioxidant activity; antibacterial activity

Introduction

In the modern era, the emergence of nanotechnology has focused on producing materials or products at the nanometric scale (1–100 nm) with controlled sizes, shapes, and structures [1]. The emergence stems from the discovery of new physicochemical properties that are advantageous and unique. These properties significantly differ from those of other materials because of their small size. This performance has led

to substantial changes across various fields, including chemistry, physics, biomedicine, biology, and pharmaceuticals [2, 3]. Inorganic nanoparticles, such as silver, gold, copper, titanium dioxide, and zinc oxide (ZnO), exhibit profound antioxidant, anti-inflammatory, antibacterial, antidiabetic, and anticancer activities [4, 5]. Zinc oxide nanoparticles (ZnO NPs) hold particular interest among these materials. In recent years, it has drawn attention from researchers due to its distinct optical and chemical behaviors, which are easily modifiable through changes in morphology. Within the broad range of metal oxide nanoparticles, ZnO NPs find applications in cutting-edge fields such as electronics, communication, sensors, cosmetics [6], environmental protection, biology, and the medicinal industry [7, 8]. Moreover, ZnO NPs demonstrate tremendous potential in biological applications, including biological sensing and labeling, gene delivery, drug delivery, and nanomedicine [8, 9], along with their antibacterial, antifungal, acaricidal, pediculocidal, larvicidal, and antidiabetic activities [10, 11].

On the contrary, several studies have indicated toxicity associated with ZnO NPs. Exposure to high concentrations of fine particles (size less than 2.5 nm in diameter) can adversely affect health by triggering respiratory and cardiovascular issues. Overexposure may result in conditions such as bronchitis or pneumonia, characterized by bluish skin tint abnormalities in liver enzymes, and diarrhea [12]. ZnO NPs are synthesized by several methods, including chemical, physical, and biological methods. While physical and chemical synthesis methods tend to be expensive and involve the use of potentially hazardous toxic solvents [6], biological synthesis using bacteria, fungi, enzymes, and plants [13, 14] offers a low-cost, rapid, and efficient alternative. This method generally leads to the formation of crystalline nanoparticles with various shapes and sizes less than 100 nm [15].

Medicinal plants serve as promising sources for creating new, safe, and biodegradable medicines [16, 17]. Using plant extracts as natural agents for reducing, capping, and stabilizing nanoparticles has made significant strides and is recognized by many researchers as an efficient green synthesis method [18, 19]. Plants are abundant in phytochemicals, particularly secondary metabolites such as alkaloids, tannins, terpenoids, phenolic, and flavonoid compounds [20], which contain functional groups such as hydroxyl (–OH), carbonyl (–CO–), and amines ($–NH_2$). These groups facilitate coupling with metal ions to form nanoparticles. Specifically, the –OH group in flavonoids plays a vital role in reducing metal ions into nanoparticles [21]. Several studies have demonstrated the synthesis of ZnO NPs using extracts of diverse plants, including lychee peel [22], *Grewia asiatica* [23], *Salvia officinalis* [24], *Pisonia Alba* [25], *Solanum torvum* L. [26], *Punica granatum* [27], *Plantain* [28], and *Anoectochilus elatus* [29]. Recent research has demonstrated the antioxidant and anti-inflammatory activities of ZnO NPs [30] using *Polygala tenuifolia* root extract. And the other studies have also highlighted antibacterial properties of ZnO NPs.

Using medicinal plant leaves, such as *Camellia sinensis*, *Scadoxus multiflorus*, and *Passiflora caerulea*, for ZnO NPs synthesis showed robust effectiveness against various bacteria, including *Pseudomonas aeruginosa*, *Klebsiella pneumoniae*, *Staphylococcus aureus*, and *Aspergillus* spp. [31]. Among plants with significant pharmacological potential, *Pistacia lentiscus* L. is widely distributed and used in Algeria for its therapeutic benefits. These benefits are closely associated with its richness in active substances [32–34]. To better understand the significance of these bioactive substances, we embarked on a study involving the synthesis of ZnO NPs using *Pistacia lentiscus* aqueous extract as a bioreducer. This study evaluated the antioxidant and antibacterial capabilities of the synthesized ZnO NPs against Gram-positive and Gram-negative human pathogenic microorganisms. Notably, this work appears to be the first of its kind in the existing literature, suggesting the use of *P. lentiscus* leaf extract as a surface stabilizer and reducing agent for ZnO NPs synthesis. The primary objective of this study was to assess the efficacy of *P. lentiscus* in the biosynthesis of ZnO NPs and their impact on antibiotic-resistant bacteria.

Materials and Methods

Plant material

The plant material used in this study comprises leaves of *P. lentiscus* L., obtained from the "virgin forest" of Misserghin, situated 5 km away from Oran in West Algeria, North Africa, in December 2022. Upon

harvesting, the leaves were cleared of branches and twigs, air-dried in shaded areas, protected from moisture, and left at ambient temperature for 10–15 days. The dried leaves were finely ground into a homogenous powder and stored in dark conditions at room temperature until further use.

Preparation of the extracts

The aqueous extract was prepared through reflux, employing 10 g of leaf powder in 100 mL of distilled water at 60–70 °C for 30 min. Following this, the crude extract was cooled and filtered using Whatman paper. This process was repeated twice using fresh solvent each time. The procedure was replicated using different ether and methanol solvents with increasing polarity. The three extracts were evaporated under vacuum at 45 °C using a rotary evaporator. The dried samples were then stored in the dark at 4 °C until they were ready for use [35].

Phytochemical study

Preliminary phytochemical analysis

Phytochemical analysis was performed to identify the active phytoconstituents in the three extracts, following standard procedures [36–40].

Determination of the polyphenolic compounds

The assessment of the total phenolic, total flavonoids, flavonols, and total tannin content in methanolic and aqueous extracts was evaluated following the methodologies described in Refs. [41–44], respectively. Gallic acid at concentrations of 40–280 μg/mL, quercetin (at concentrations of 40–100 μg/mL), quercetin (at concentrations of 20–100 μg/mL), and catechin (at concentrations of 200–1 000 μg/mL) were used as standards. These results are presented as milligrams of gallic acid, quercetin, and catechin equivalents per 1 g of dry weight sample (mg GAE/g DM, mg QE/g DM, and mg CE/g DM, respectively).

Synthesis of ZnO NPs

The synthesis of ZnO NPs followed the method described in Ref. [45]. Initially, an aqueous extract was prepared by combining 10 g of vegetal powder of *P. lentiscus* leaves with 200 mL of distilled water, heated for 30 min at 60–70 °C, left to cool at room temperature (25 ± 2 °C), filtered using N2 filter paper, and stored at 4 °C for future use. Subsequently, 15 mL of this aqueous extract was added to 285 mL of 0.1 mol/L zinc acetate dihydrate ($Zn(CH_3COO)_2$, $2H_2O$), heated at 78 °C for 30 min, and titrated with 1 mol/L NaOH solution until the pH value was 12. Following this, continuous stirring was performed for 4 h at the same temperature to form *P. lentiscus*-derived ZnO NPs (Pl–ZnO NPs). To remove impurities, the Pl–ZnO NPs were washed by several centrifugations at 4 000 r/min for 5 min. The resulting sample was then heated in an air-heated furnace at 70 °C overnight. A light white powder was obtained by further heating the powder in a muffle furnace at 500 °C for 2 h and stored for characterization [46].

Characterization of the Pl–ZnO NPs

Ultraviolet–visible (UV–Vis) analysis

This technique is based on the transition of valence electrons from their fundamental state to an excited state prompted by an electromagnetic wave. This transition involves the rotational and vibrational properties of molecules, necessitating relatively high energy levels that correspond to the UV–Vis wavelength range. The UV–Vis energy spectrum within the electromagnetic spectrum covers 1.5–6.2 eV, corresponding to a wavelength range of 800–200 nm [47]. The optical properties of the Pl–ZnO NPs were determined using UV–Vis spectrometry (6715 Spectrophotometer JENWAY) at room temperature. Spectral analysis was performed at a resolution of 1 nm in the 200– 800 nm range.

FTIR analysis

The confirmation of the material's functional groups was achieved using a Fourier Transformation Infrared spectrometer (Agilent Technologies Cary 630 FTIR) operating in the transmittance mode within the range of 4 000–500 cm^{-1}. The primary instrument is connected to a microscope, enabling the analysis of small sample areas. In the analysis of Pl–ZnO NPs, the powder is placed under the microscope, causing a shift in the energy of the laser photons either upward or downward. This shift in energy provides valuable information about the vibration modes within the system. Identification of these connections is achieved using their corresponding wave numbers. Typically, stronger bonds and lighter atoms exhibit higher stretching frequencies (wavenumbers) [48].

X-ray diffraction (XRD)

The XRD is a method that enables the identification of crystallized phases within a sample and the

determination of the arrangement of atoms along with their interatomic distances [49]. To analyze the structure and grain size of ZnO, XRD techniques were employed using an X-ray diffractometer (Rigaku Miniflex 600) equipped with a Cu-*K*α (λ = 1.540 6) within the 2θ angles ranging from 20° to 70°. The X-rays were generated at 30 kV and 20 mA.

Scanning electron microscopy (SEM)

The shape and morphology of the PI–ZnO NPs were determined by SEM and energy-dispersive X-ray spectroscopy (EDS). This technique involves systematically scanning the sample's surface, enabling high magnification and improved depth of field to represent morphological features. When coupled with X-ray analysis, it potentially allows for chemical examination. SEM functions by emitting electrons from an energy E_0 cathode and detecting signals generated by the interaction between these electrons and the sample [50].

Antioxidant activity

DPPH radical trapping test

The assessment of the *in vitro* antioxidant potential of *P. lentiscus* L. extracts and Pl–ZnO NPs on the 2,2-diphenyl-1-picrylhydrazyl (DPPH) radical followed the method described by Blois [51].

Reduction of the DPPH free radical by TLC bioautography

The various extracts (etheric, methanolic, aqueous, and Pl–ZnO NPs) were applied at an equal concentration (50 µg/mL) onto a silica gel F_{254} thin layer plate. Subsequently, these plates were sprayed with a DPPH solution (0.004% in methanol) and observed after 30 min of drying at 60 °C. A positive test is indicated by the appearance of yellow spots against a purple background [52].

Reduction of the DPPH free radical by spectrophotometric assay

This method involves extracts that exhibited positive antiradical activity through bioautography. It followed the procedure outlined in Ref. [53]. A 1.9 mL DPPH solution, previously prepared by dissolving 4 mg of DPPH in 100 mL of methanol, was combined with 100 µL of each extract at various concentrations (200, 300, 400, 500, 600 µg/mL). After a 30 min incubation period, absorbance was measured at 517 nm against a blank (DPPH/methanol). Ascorbic acid, quercetin, and butylated hydroxytoluene (BHT), which were prepared under the same conditions at different concentrations, served as standard antioxidants. The results were expressed as the percentage inhibition of DPPH, which was calculated using the equation demonstrated below. The ability of *Pistacia lentiscus* L. extract to neutralize the DPPH radical was quantified as the IC_{50} value (µg/mL), representing the concentration necessary for 50% inhibition [54]:

$$I\,(\%) = \frac{A_0 - A}{A_0} \times 100$$

where I (%) is the percentage of inhibition, A_0 is the absorbance of DPPH solution without extract, and A is the absorbance in the presence of extract or standard.

Antibacterial activity of the Pl–ZnO NPs

The antibacterial activity of synthesized ZnO NPs, ether, methanol, and aqueous solutions are assessed by the disk diffusion method [55] targeting four bacterial strains: two Gram-positive bacteria, *Staphylococcus aureus* (ATCC 6538) and *Bacillus cereus* (ATCC 10876), and two Gram-negative bacteria, *Escherichia coli* (ATCC 8739) and *Pseudomonas aeuroginosa*. The pathogenic microorganisms were separately cultured in nutrient broth and then incubated at 37 °C for 18 h until they reached a density equivalent to a turbidity of 0.5 Mc-Farland standards (10^8 CFU/mL). Subsequently, 100 µL of the pathogenic cultures were swabbed onto Muller–Hinton agar (MHA) plates after overnight growth in a Petri dish. Different concentrations of 100, 300, 500, 700, and 900 mg/mL of ZnO NPs, along with ether, methanol, and aqueous extracts dissolved in dimethylsulfoxide (DMSO), were placed onto a filter paper disk and allowed to dry before being placed on the agar. DMSO served as the control. The plates underwent a pre-diffusion of 1 h at 4 °C before incubation at 37 °C for 24 h. Each extract was tested in triplicate, and the resulting inhibition zone diameters were measured for analysis.

The results were expressed according to Ref. [56]:
$D \leq 8$ mm: resistant strain.
9 mm $\leq D \leq$ 14mm: susceptible strain.
$D >$ 15 mm: very susceptible strain.

Determination of minimum inhibitory concentration (MIC)

To assess the antibacterial activity, we conducted an

MIC assessment, focusing only on bacteria displaying sensitivity to the different extracts. Following the guidelines outlined in Ref. [57], the MIC determination involved dissolving Pl–ZnO NPs, ether, methanol, and aqueous extracts in DMSO at decreasing concentrations (100–0.78 mg/mL). In this protocol, 100 µL of each extract was added to individual microcentrifuge tubes within the experimental series, along with 20 µL of a bacterial suspension prepared in 900 µL of Mueller–Hinton broth. A specific tube was used as a negative control, containing the broth culture and inoculum prepared under the same conditions. After a 24 h incubation period at 37 °C, the results were assessed by observing any changes in turbidity and comparing them with the turbidity of the control tube.

Determination of minimum bactericidal concentration (MBC)

MBC represents the concentration of the antibacterial substance required to achieve a reduction of 0.01% germs after 18–24 h of incubation at 37 °C [58]. To initiate, 0.1 mL of the pre-culture was diluted in a separate tube containing 10 mL of Mueller–Hinton broth, forming the initial inoculum of the 100-fold dilution. This was then further diluted using a geometric progression ratio (10^{-1}–10^{-4}, v/v). Subsequently, these various dilutions are inoculated onto a MHA plate with streaks of 5 cm length using a calibrated loop of 0.2 µL (Box A). The dilutions of 100, 10^{-1}, 10^{-2}, 10^{-3}, and 10^{-4} correspond to survival rates of 100%, 10%, 1%, 0.1%, and 0.01%, respectively [59]. Tubes without observed turbidity (the tubes used to determine the MIC) were used to inoculate MHA (Box B) with 5 cm-long streaks using a calibrated 0.2 µL loop, starting with the tube corresponding to the MIC. Boxes A and B were then incubated at 37 °C for 18–24 h. Subsequently, the number of colonies on the streak at a 10^{-4} dilution from Box A was compared with each streak of Box B. According to Ref. [60], the MBC/MIC ratio aids in determining the bactericidal and bacteriostatic properties of the studied extract:

- If the MBC/MIC ratio ≤ 4, the substance tested is bactericidal.
- If the MBC/MIC ratio > 4, the substance tested is bacteriostatic.

Statistical analysis

The experiments were performed in triplicate, and the results were determined using the mean ± SEM and analyzed using GraphPad Prism (version 5). Analysis of variance was performed using the analysis of variance (ANOVA) test. Tukey's test was employed to identify significant differences between means. Therefore, significance was established at $P = 0.05$.

Results and Discussion

Yield of extracts from leaves of *Pistacia lentiscus* L.

The percentage-based quantitative assessment of extraction yields varies because of the use of diverse organic solvents. Among these, the aqueous raw extract stands out, with the highest yield rate at 33%. This high yield is attributed to its capacity to dissolve the maximum amount of bioactive compounds. Conversely, the methanolic extract showed an average yield of 16.7%, while the etheric extract exhibited the lowest yield of 6.8%. This finding suggests that solvents with higher polarity tend to generate the best yields, aligning with previous studies, such as those by Refs. [61, 62], which reported hydromethanolic extract yields of 37.34% and 23.5% in distinct regions of Morocco and the northwest of Tunisia, respectively. Cherbal et al. [63] observed a yield of (44.58 ± 1.76)% for the hydromethanolic extract of the leaves of *P. lentiscus* harvested in Jijel (East of Algeria). Alternatively, the work of Ref. [64] recorded much lower yield rates for ethanolic extracts at 6.09% for leaves and 3.07% for fruits. The extraction yield depends on the nature and polarity of the solvent extraction techniques, pH, temperature, solvent mass/volume ratio, time intervals, number of extraction steps, sample particle size, chemical composition of compounds, and the presence of interfering substances [65].

Phytochemical studies

Extracts obtained from *P. lentiscus* leaves using ether, methanol, and water were analyzed for various phytoconstituents, as shown in Table 1. The results reveal the abundance of bioactive molecules in this plant. The use of polar solvents resulted in extracting a wide array of phytoconstituents, including phenolic compounds, flavonoids (flavanones and flavanols), catechin tannins, saponins, salt alkaloids, coumarins, sterols and steroids, steroidal and triterpene glycosides, and cardiac glycosides. Additionally, the

Table 1 Results of phytochemical screening

Test for	Etheric extract	Methnolic extract	Aqueous extract
Basic alkaloids	–	ND	ND
Emodols	+	ND	ND
Terpenoids	–	ND	ND
Free quinones	+	ND	-
Fatty acid	+	ND	ND
Phenolic compounds	ND	+	+
FlavonoidsFlavanones / flavanols	ND	+	+
Gallic and catechic tannins	ND	+	+
Alkaloids salts	ND	–	ND
Coumarins	ND	+	ND
Sterols and steroids	ND	+	ND
Glycosides steroid and triterpene	ND	+	ND
Reducing compounds	ND	+	ND
cardiotonics Glycosides	ND	+	ND
Saponosides	ND	ND	+
Anthocyanins	ND	ND	–
Combined anthraquinonsO–glycosidesC–Glycosides	NDND	NDND	+–

Note : +, presence; −, absence; ND, not determined.

etheric extract indicated the presence of emodols, free quinones, and fatty acids.

Determination of total polyphenol, flavonoids, flavonols, and condensed tannins content

The total contents of polyphenols, flavonoids, flavonols, and condensed tannins in methanolic and aqueous extracts were obtained from calibration curves. These curves were established using increasing concentrations of gallic acid, quercetin, and catechin, expressed as mg of gallic acid equivalent per gram of dry matter weight (mg EAG/g DM), mg of quercetin equivalents per gram of dry matter weight (mg EQR/g DM), and mg of catechin equivalent per gram of dry matter (mg EC/g DM). The results of the determination of total polyphenols, flavonoids, flavonols, and tannins in the methanolic and aqueous extracts are shown in Fig. 1.

From these results, it is evident that the highest concentrations were observed in total polyphenols (353.97 ± 8.28) mg/g and (246.07 ± 5.62) mg/g, followed by flavonoids with concentrations of (71.94 ± 1.56) mg/g and (56.32 ± 0.92) mg/g for the aqueous and methanolic extracts, respectively. Conversely, tannins exhibited an average rate of (22.31 ± 1.97) mg/g for the aqueous extract and (34.75 ±1.63) mg/g

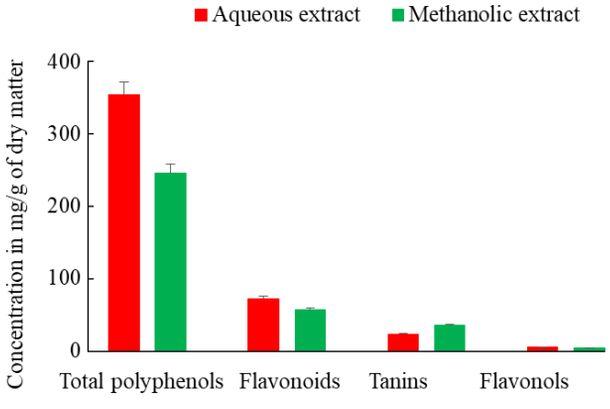

Fig. 1 The total contents of polyphenols, flavonoids, tannins, and flavonols found in the aqueous and methanolic extracts from the leaves of *Pistacia lentiscus* L.

for the methanolic extract. The lowest content was found in flavonols, measured at (4.69 ± 0.57) mg/g and (3.34 ± 0.66) mg/g for the aqueous and methanolic extracts, respectively. Our findings are comparable to those of Bampouli [66], demonstrating that the total content of phenolic compounds for the leaves of *P. lentiscus* is the highest; for the fresh leaves, it varies from (147.99 ± 0.01) to (314.88 ± 0.01) mg Eq FA/g of dry extract, whereas for the dried leaves, value varies from (125.33 ± 0.01) to (269.70 ± 0.01) mg Eq FA/g of dry extract. The aqueous extracts showed the highest amount with

values of (314.88 ± 0.01) and (271.03 ± 0.00) mg Eq AG/g of dry extract, which indicates that water is considered the most suitable solvent for the extraction of phenolic compounds. Our analysis of the flavonoid content indicates a lower concentration compared with the findings in Ref. [67]. This confirms that the primary concentration of flavonoids in the extracts of *P. lentiscus* leaves is predominantly in the ethyl acetate fraction of the ethanolic extract, measuring (278.507 ± 0.377) mg Eq rutin/g DM. Our results contradict the observations of Ref. [68], who reported lower flavonoid content in the leaves of *P. lentiscus*, (3.107 ± 0.014) mg/g and (8.218 ± 0.009) mg/g, respectively, for the aqueous and ethanolic extracts. Similar studies by Ref. [63] reported values of 38.7 ± 0.020 and 12.6 ± 4.1 mg/g for the methanolic extract of the same species. Regarding flavonols, the notably low content in the aqueous and methanolic extracts might be attributed to the heterogeneous nature of flavonoids, which are present in various classes with differing solubilities in polar and apolar solvents [69]. Our findings on the tannin content in the leaves of *P. lentiscus* differ from those in Ref. [70], who recorded a higher tannin content estimated at 997.8 mg Eq tannic acid/g DM for the leaves of the same plant. These variations in polyphenols, flavonoids, flavonols, and tannins may be due to the biotope of the plant west or east of Algeria, interspecific variations, and/or the harvest stage, storage period, and equipment for extracting these compounds.

Green synthesis of ZnO NPs

Synthesis process

In this study, we synthesized ZnO NPs using the aqueous extract of *Pistacia lentiscus* leaves as phytoreducing agents for Zn ions. Upon incineration in the muffle furnace (Fig. 2), we observed an immediate shift from pale yellow to dark brown, resulting in the production of dry white powder. This transformation in color serves as a distinct indication of Zn ion bioreduction, leading to the subsequent formation of ZnO NPs.

Characterization by ultraviolet spectroscopy

The UV–Vis absorption spectrum of the Pl–ZnO NPs displays a characteristic maximum absorption peak of ZnO, centered around 310 nm (Fig. 3), indicating the likely formation of ZnO [71]. There was an observable increase in the intensity of the peak concerning the concentration of zinc acetate. This may be attributed to the growing quantity of nanoparticles formed through the transformations of Zn ions, likely caused by the complete extraction of (Zn ions) by the extract. Our results align closely with those of Ref. [72], where they recorded an absorption

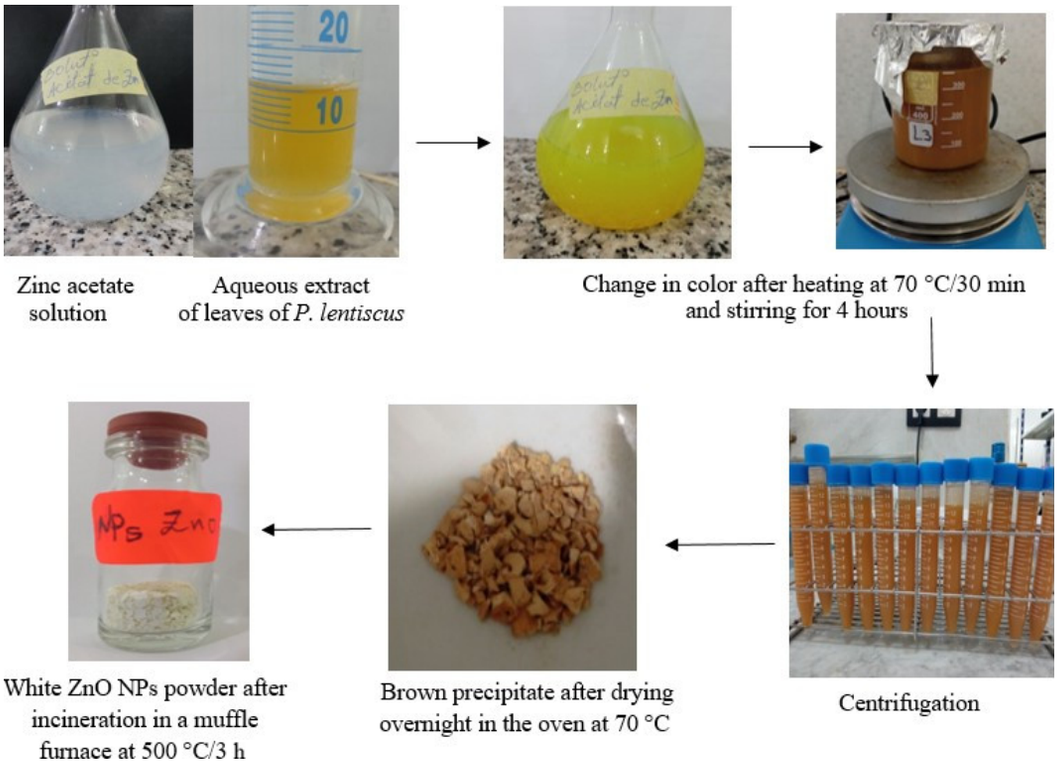

Fig. 2 Biosynthesis process of zinc oxide nanoparticles from the aqueous extract of *P. lentiscus* L.

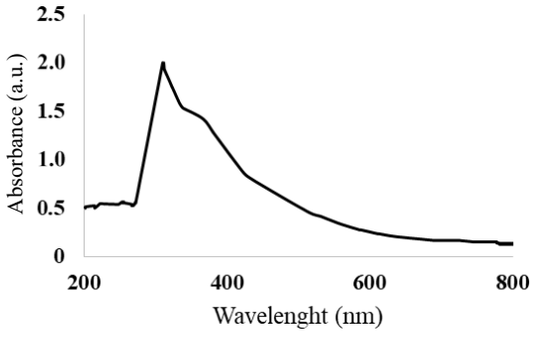

Fig. 3 Ultraviolet spectrum of ZnO NPs synthesized using the leaf extract of *Pistacia lentiscus* L.

peak of 303 nm for the zinc acetate solution derived from broccoli and 320 nm for the ZnO solution without broccoli.

Characterization by infrared spectroscopy

Infrared spectroscopy allows us to analyze the vibration modes of bonds within ZnO and the organic surface layer, providing insights into the functional groups of nanoparticles. These results are illustrated in Fig. 4. Three distinct zones emerge, displaying absorbance bands associated with alkyne chains (to the stretching vibration mode at 2 260–2 100 cm^{-1}) [73], groups (C−O) from alcohols (1 250–970 cm^{-1}) [74], to (Zn−O) bonds (800–400 cm^{-1}) in ZnO [75]. With ZnO NPs synthesized and annealed at 500 °C, the presence of an adsorption peak at 680 cm^{-1} suggests the synthesis of ZnO NPs through the green route [76].

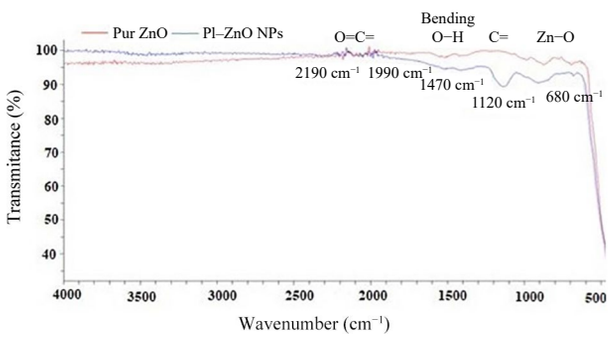

Fig. 4 FTIR spectrum of Pl–ZnO NPs synthesized from *P. lentiscus* L. leaves compared to pure zinc oxide (industrial).

Characterization by XRD

The XRD results of the synthesized ZnO NPs annealed at 500 °C, derived from a 0.1 mol/L zinc acetate concentration, are presented in Fig. 5.

The sample spectrum exhibits distinct diffraction peaks throughout, aligning well with various crystal blueprints such as (100), (002), (101), (102), (110), (103), (200), (112), (004), and (202), corresponding

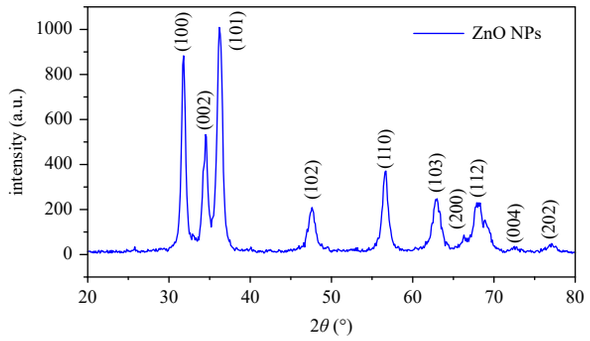

Fig. 5 The X-ray diffraction spectra of the Pl–ZnO NPs synthesized from *P. lentiscus* L leaves.

to the hexagonal würtzite structure of ZnO consistent with the JCPDS card number (No. 36-1451 for ZnO) [77, 78], which corroborates Musarrat findings [79]. Notably, the presence of peaks (100), (002), and (101) in the XRD spectrum indicates the high-purity crystallization of ZnO NPs. The absence of peaks related to other impurities suggests complete conversion of the Zn precursor into ZnO NPs. Compounds such as phenols and flavonoids from *P. lentiscus* leaf extract serve as both a reducing agent and a protective layer for the outer surface of zinc acetate molecules, facilitating the formation of ZnO NPs. The distinct, narrow, and prominent diffraction peaks suggest that the product's particles have a well-defined crystalline structure. The high intensity of these peaks indicates the high crystallinity of the produced ZnO NPs. Additionally, the Scherrer formula was used to estimate the crystallite size (D) [80].

$$D = k\lambda/\beta\cos\theta$$

where k is the Scherrer's constant (k = 0.94), λ is the wavelength of the X-ray radiation (1.540 6 Å), θ is the Bragg's angle of the peak and β is FWHM (in radium). This XRD analysis proves *P. lentiscus* leaves are effective reducing agents for synthesized ZnO NPs. Particles were determined to have diameters in the 33.90 nm range.

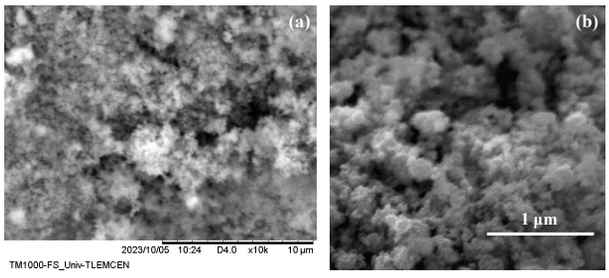

Fig. 6 Scanning electron microscopy images of ZnO nanoparticles: **(a)** 0.1 mol/L and **(b)** 0.1 mol/L (focused image).

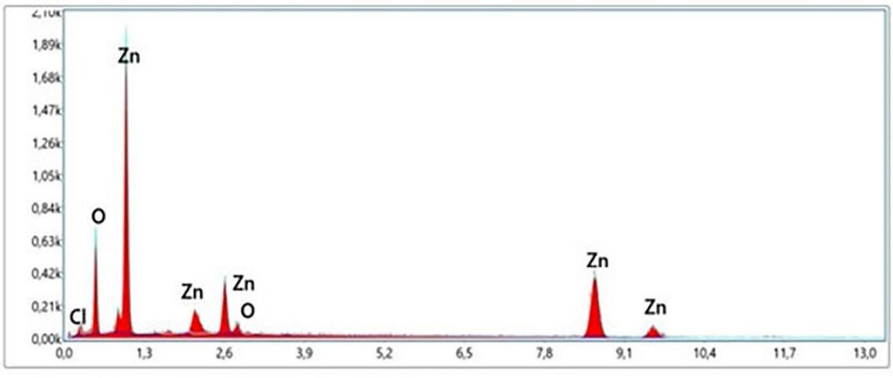

Element	Masse (%)	Atomique (%)	Intensite totale	Error (%)	Kratio	Z	A	F
O	22.71	52.13	44.80	9.87	0,0795	1.2067	0.2900	1.0000
Cl	9.39	9.73	37.29	5.70	0,0728	1.0366	0.7432	1.0067
Zn	67.90	38.15	69.85	3.36	0,6229	0.9101	1.0025	1.0056

Fig. 7 Energy-dispersive X-ray spectroscopy spectra of synthesized ZnO NPs.

SEM of ZnO NPs

SEM images were used for predicting the shape of ZnO NPs, with varying magnifications displayed in Figs. 6(a) and 6(b). The majority of these ZnO NPs exhibit an aggregated, dried cotton-like appearance. Further analysis using EDS presented in Fig. 7 confirms the presence of Zn and O in the ZnO NPs, indicating approximate weight percentages of approximately 38.15% for Zn and 52.13% for O.

Evaluation of biological activities of extracts of *P. lentiscus* L.

TLC bioautography

The antioxidant activity test conducted via TLC bioautography of various extracts (etheric, methanolic, aqueous, and Pl–NPs ZnO) at a concentration of 50 µg/mL, compared with two controls (ascorbic acid and quercetin) at a concentration of 25 µg/mL, revealed yellow spots on a purple background when exposed to DPPH, which indicates the ability of these substances to reduce the DPPH radical.

Reduction of DPPH by spectrophotometric assay

The effectiveness of antiradical activities is represented through percentage inhibition values and IC_{50} expressed in µg/mL for the etheric, methanolic, aqueous, and Pl–ZnO NPs extracts. These values are compared with the standards: ascorbic acid, quercetin, and BHT using graphical analysis performed with the software "GraphPad prism 5" (Fig. 8).

The antiradical activity profile from the four extracts of *P. lentiscus* leaves indicates a concentration-dependent antioxidant potential. This signifies that the antiradical percentage increases as the concentration of the extracts rises. Notably, the methanol extract exhibited high antiradical potential with an IC_{50} of (16.72 ± 1.72) µg/mL, whereas the

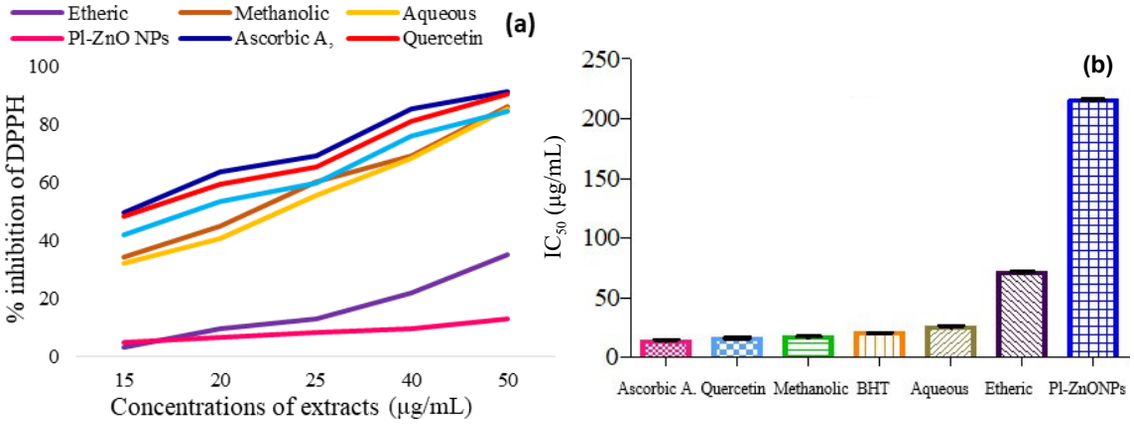

Fig. 8 Antioxidant activity **(a)** Percentage of DPPH inhibition **(b)** IC_{50}.

aqueous extract exhibited an IC_{50} of (25.37 ± 1.92) µg/mL, compared with the three standards: IC_{50} of (13.73 ± 2.11), (15.89 ± 0.97), and (20.50 ± 0.16) µg/mL for ascorbic acid, quercetin and BHT. The etheric extract showed an average antioxidant power with an IC_{50} of 70.80 ± 1.50 µg/mL, and the Pl–ZnO NPs demonstrated low antioxidant activity with an IC_{50} of (215.53 ± 1.04) µg/mL. These results highlight the substantial antioxidant activity of the methanolic and aqueous extracts of *Pistacia lentiscus* L. leaves, reaching maximum percentages of antiradical activity at 86.49% and 85.32%, respectively at a concentration of 50 µg/mL. Conversely, the etheric and Pl–ZnONPs extracts showed lower antioxidant activity, demonstrating percentages of inhibition of the DPPH radical at 35.36% and 12.92%, respectively, at the concentration of 50 µg/mL. Our results are in agreement with the work of Refs. [81, 82] who reported very high antioxidant activity of the methanolic and aqueous extracts of *P. lentiscus* leaves. Another study in Ref. [83] showcased the remarkable antioxidant effect of the methanolic, ethanolic, and aqueous extracts from different parts of *P. lentiscus* against the DPPH radical. The aqueous extract of the leaves demonstrated an IC_{50} of (9 ± 0.37) µg/mL. The robust antioxidant potential of the methanolic and aqueous extracts can be attributed to the presence of polyphenols, flavonoids, and tannins in the leaves of *P. lentiscus*, as quantitatively assessed in previous studies. These substances are recognized as antioxidants capable of neutralizing radical and reactive oxygen species [84]. Polyphenols act as efficient hydrogen atom donors to the DPPH radical because of their optimal chemical structures [85]. Phenolic compounds in plants readily donate electrons or protons to neutralize free radicals, significantly contributing to their strong antioxidant activity [86]. Further studies on the relationship between the chemical structure of phenolic compounds and their ability to scavenge free radicals have emphasized the importance of the number, position, and nature of the B and C ring substitutes, as well as the degree of polymerization [87].

Evaluation of antibacterial activity

The bacterial strains (*Staphylococcus aureus*, *Bacillus cereus*, *Escherichia coli*, and *Pseudomonas aeruginosa*) were initially identified through microscopic observation in their fresh state to determine their shape and mobility. Subsequently, confirmation was performed using Gram staining.

Disk method (aromatogram)

Our results indicated inhibition zones ranging from 6 to 24 mm. These varying diameters were observed across different strains, signifying their sensitivity or resistance, which was influenced by the concentration of the extract used (Figs. 9–12).

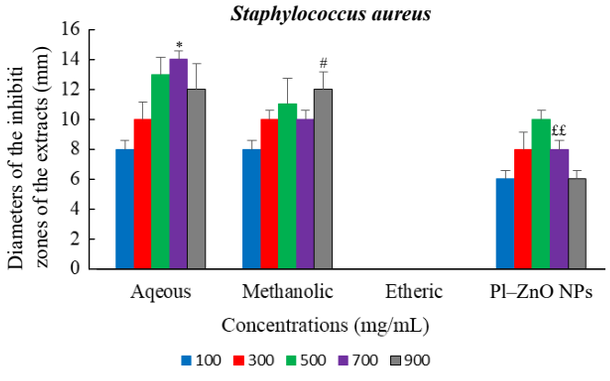

Fig. 9 Inhibition zone diameters (mm) of crude extracts and ZnO NPs from *P. lentiscus* leaves against *S. aureus*. The reported values represent means and their respective standard errors (X ± ES). The symbols (*, #, £) indicate statistically significant differences (ANOVA test). Specifically, * denotes a significant difference between the aqueous and methanolic extracts at a concentration of 700 mg/mL (*p < 0.05). # denotes a significant difference between the methanolic extract and ZnO NPs at a concentration of 900 mg/mL (# p < 0.05). £ denotes a significant difference between the aqueous extract and Pl–ZnO NPs at a concentration of 700 mg/mL (£p < 0.01).

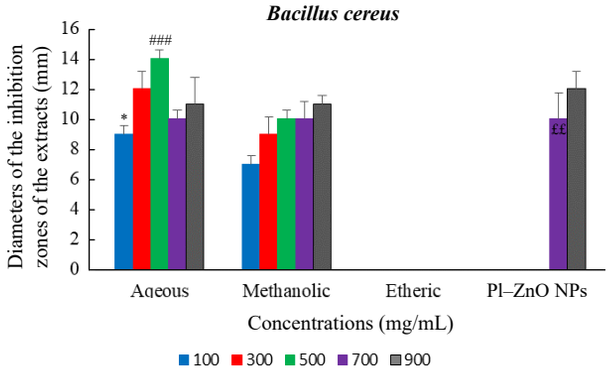

Fig. 10 Inhibition zone diameters (mm) of crude extracts and Pl–ZnO NPs derived from *P. lentiscus* leaves against *Bacillus cereus*. The symbol * denotes a significant difference between the aqueous and methanolic extracts at a concentration of 100 mg/mL (*p < 0.05). The symbol # denotes a significant difference between the aqueous and methanolic extracts at a concentration of 500 mg/mL (### p < 0.0001).

The Pl–ZnO NPs exhibited the largest diameter, demonstrating significant activity against the *E. coli* strain with a zone of inhibition measuring (24 ± 1)

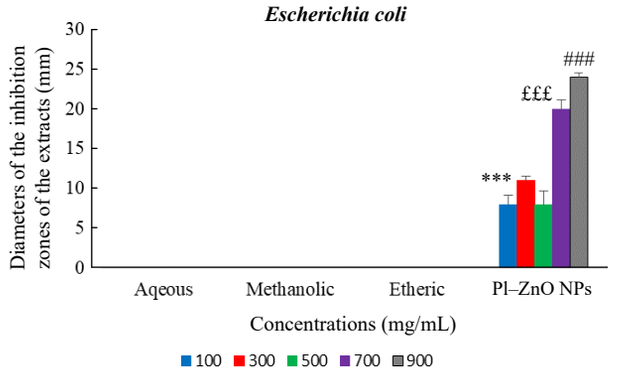

Fig. 11 Inhibition zone diameters (mm) of crude extracts and Pl–ZnO NPs obtained from *P. lentiscus* leaves against *E. coli*. The symbol * denotes significant difference between the aqueous extract and Pl–ZnO NPs at a concentration of 100 mg/mL (***p < 0.000 1); The symbol £ denotes significant difference between the aqueous extract and ZnO NPs at a concentration of 700 mg/mL (£££ p < 0.000 1); and # denotes a significant difference between the methanolic extract and Pl–ZnO NPs at a concentration of 900 mg/mL (### p < 0.0001).

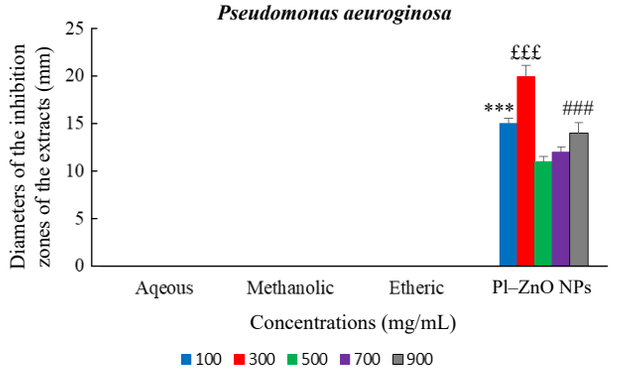

Fig. 12 Inhibition zone diameters (mm) caused by crude extracts and Pl–ZnO NPs from *P. lentiscus* leaves against *P. aeruginosa*. The comparisons indicate significant difference between the aqueous extract and Pl–ZnO NPs at a concentration of 100 mg/mL (***p < 0.000 1); the methanolic extract and ZnO NPs at a concentration of 300 mg/mL (£££ p < 0.000 1); and the aqueous extract and Pl–ZnO NPs at a concentration of 900 mg/mL (### p < 0.000 1).

mm at a concentration of 900 mg/mL. This was followed by *P. aeruginosa*, which displayed an inhibition diameter of (20 ± 2) mm at a concentration of 300 mg/mL. However, these strains were resistance to etheric, methanolic, and aqueous extracts. *S. aureus* showcased diameters ranging from (6 ± 1) mm to (10 ± 1) mm at concentrations of 100 and 500 mg/mL against ZnO NPs. A sensitivity in the *Bacillus cereus* strain was observed toward aqueous and methanolic extracts, revealing inhibition zones varying from (9 ± 1) to (14 ± 1) mm and from (7 ± 1) to (11 ± 1) mm at concentrations of 100 and 500 mg/mL and 100 and 900 mg/mL, respectively. ZnO NPs displayed two zones of inhibition at concentrations of 700 and 900 mg/mL, measuring (10 ± 3) and (12 ± 2) mm, respectively. Conversely, *B. cereus* exhibited resistance against the etheric extract. Comparatively, our results indicate that *S. aureus* and *B. cereus* are more sensitive to aqueous, methanolic, and etheric extracts than *E. coli* and *P. aeruginosa*. This sensitivity could be attributed to differences in the cell wall structure between Gram-positive and Gram-negative bacteria [88]. Our results contradict the work of Ref. [89], which claims that Gram-positive bacteria are more resistant to antimicrobial agents because of variations in the chemical composition of their cell walls. Gram-negative bacteria possess a wall that allows the penetration of lipophilic molecules because of the presence of lipopolysaccharides (LPS) with negative charges, facilitating the adhesion of NPs. Conversely, Gram-positive bacteria primarily consist of peptidoglycans, which allow the passage of hydrophilic molecules [90]. Our results are consistent with the findings of Ref. [91], where Pl–ZnO NPs biosynthesized using *Bauhini tomentosa* leaf extract displayed antibacterial effects across all tested bacterial strains. The bactericidal effect of Pl–ZnO NPs was notably higher for Gram-negative bacteria than for Gram-positive bacteria, which was influenced by structural composition differences [92]. The reported zones of inhibition exhibited notable diameters for *P. aeruginosa* (20.3 mm), *E. coli* (19.8 mm), *B. subtilis* (8.1 mm), and *S. aureus* (10.7 mm). Our results align with the research conducted by [93], which studied the antimicrobial activity of Pl–ZnO NPs against pathogenic microorganisms using the agar diffusion technique. The most substantial zones of inhibition were observed against *B. subtilis* (24 mm), *E. coli* (24 mm), *S. aureus* (22 mm), and *P. aeruginosa* (22 mm). Similarly, Ref. [94] examined the effect of three concentrations (20, 30, and 40 µg/mL) of Pl–ZnO NPs against three *Pseudomonas aeruginosa* isolates using the agar diffusion technique. Their results revealed an average zone of inhibition of 19.7 mm at a concentration of 20 µg/mL. However, concentrations of 30 and 40 µg/mL exhibited inhibition zones of 22.4 and 33.2 mm, respectively. These results confirm the antibacterial activity of Pl–ZnO NPs, indicating that increased concentrations lead to larger zones of inhibition. The antimicrobial efficacy of ZnO NPs may be associated with their size, allowing them to assess cells through transmembrane protein. Upon attachment to bacterial cells, structural alterations occur, blocking transport

channels [95]. This entire process is contingent on the size of the NPs. Smaller NPs, which are 250 times smaller than a bacterium, are more effective. They adhere to the (-SH) groups of wall proteins, penetrating the membrane, alternating permeability, and resulting in cell lysis [96–98]. In contrast, larger NPs possess a larger absolute surface area, enhancing their adhesion capacity through van der Waals forces. Subsequently, NPs are capable of internalization, generating ionization within the cell and causing damage to intracellular structures, ultimately resulting in cellular death [99]. The production of reactive oxidizing species (ROS) by metal NPs has been identified as a possible mechanism behind their bactericidal activity, which plays an important role in their effectiveness against bacteria. These highly reactive species can damage peptidoglycans, cell membranes, DNA, mRNA, ribosomes, and proteins [98]. Additionally, ROS can impede transcription, translation, and enzymatic activity and disrupt the electron transport chain. For certain metal oxide NPs, the generation of ROS is the primary mechanism of their toxicity [100, 101]. Metal oxides NPs also possess the capability to deactivate proteins and damage DNA. Metal atoms tend to bind to the thiol group of enzymes, subsequently deactivating their functions. Moreover, there is a suggestion that metal ions attach themselves between pyrimidine and purine base pairs, disrupting hydrogen bonding between the two antiparallel strands and destroying the DNA molecule. Although further investigation is needed, metal ions tend to attach to DNA once they enter the cell [102, 103].

According to Liu et al. [104], the treatment of *E. coli* with ZnO nanoparticles resulted in particle adherence to the cell membrane, causing membrane deformation and disruption of intracellular structures. Kadiyala et al. [95] investigated the antibacterial impact of ZnO nanoparticles on multidrug-resistant *S. aureus* and concluded that the formation of ROS alone might not be the predominant antibacterial mode of action. However, elevated concentrations of Zn ions in nanostructures disrupt virulence by inhibiting crucial glycolytic enzymes, thereby reducing hyaluronic acid capsule synthesis. Consequently, this alteration leads to a shift in the expression of carbon catabolic pathways [95]. Overall, these results are highly encouraging and promising. *E. coli* and *P. aeruginosa* strains, initially resistant to the tested extracts and numerous antibiotics, exhibited increased sensitivity to the Pl–ZnO NPs. This discovery suggests the potential importance of testing other strains within the same species that display higher resistance. Comparing the antibacterial activity results obtained from Pl–ZnO NPs with the crude extracts (etheric, methanolic, and aqueous) of *Pistacia lentiscus* leaves, it was observed that the biosynthesized NPs were the most effective extract against the bacterial strains, mainly exhibiting potency against gram-negative bacteria.

Determination of MIC and MBC

We observed that the aqueous extract, methanol, and Pl–ZnO NPs showed a bactericidal effect against *Staphylococcus aureus*, as indicated by a MBC/MIC ratio of 1. We observed a similar bactericidal effect of the aqueous extract against *Bacillus cereus*. However, the methanolic extract displayed a bacteriostatic effect on *Bacillus cereus*, as evidenced by a MBC/MIC ratio of 8. The ZnO NPs showed a bactericidal effect on *Pseudomonas aeruginosa* with a MBC/MIC of 2.

Conclusions

This study introduces a more eco-friendly technique for synthesizing ZnO NPs by extracting their bioactive components from *P. lentiscus* leaves. This method is simple, environmentally friendly, nontoxic, and biologically driven. The optical and structural properties were assessed using UV–Vis spectroscopy, FTIR, and XRD. UV–Vis spectroscopy confirmed the synthesis of ZnO nanoparticles, revealing their formation with an absorption peak at 310 nm. FTIR spectra confirmed the presence of functional groups in ZnO, while X-ray analysis exhibited well-defined peaks on planes (002), (100), and (101), indicating a hexagonal structure (würtzite) (JCPDS-file: 36-1451) with good crystalline quality and a grain size of 33.90 nm. Examining the nanoparticle morphology through SEM with EDS demonstrated the ZnO nanoparticle's resemblance to dried cotton, with EDS confirming the presence of Zn and O. Comparison of biological activities between ZnO NPs and etheric, methanolic, and aqueous crude extracts yielded 6.80%, 16.70%, and 33%, respectively. Phytochemical screening revealed the abundance of polyphenols, flavonoids, tannins, sterols, steroids, steroidal and triterpene glycosides, coumarins, and saponosides in the plant. Specifically, the aqueous

and methanolic extracts contained polyphenols (353.97 ± 8.28 and 246.07 ± 5.62 mg/g), flavonoids (71.94 ± 1.56 and 56.32 ± 0.92 mg/g), flavonols (4.69 ± 0.57 and 3.34 ± 0.66 mg/g), and tannins (22.31 ± 1.97 and 34.75 ± 1.63 mg/g), respectively. Regarding antioxidant activity, the methanolic extract exhibited the highest antiradical potential (IC_{50} = (16.72 ± 1.72) µg/mL), followed by the aqueous extract (IC_{50} = (25.37 ± 1.92) µg/mL), whereas etheric extracts and ZnO NPs showed weak antioxidant activity. Additionally, ZnO NPs displayed antibacterial activity against *Escherichia coli* and *Pseudomonas aeruginosa* strains, suggesting their potential application in the biomedical field for surface decontamination.

CRediT Author Statement

Rihab Haddi: Conceptualization, methodology, experiments (SEM, XRD), software, results analysis, writing–reviewing, and editing. **Aicha Maria El Kharraz, Mimouna Ikram Kerroumi:** Experiments (phytochemical screening, assessment of biological proprieties).

Acknowledgements

The authors thanks physics departement of Tlemcen University, Algeria. Also Prof. LAOUINI Sallah Eddine, Laboratory of Valorization and Technology of Saharian Resources, Departement of Process Engineering, Faculty of Technology, Hamma Lakhdar University, El-Oued, 39000 Algeria.

Conflict of Interests

The authors declare that no competing interest exists.

References

[1] N. Senthilkumar, E. Nandhakumar, P. Priya, et al. Synthesis of Zno nanoparticles using leaf extract of Tectona grandis (L.) and their antibacterial, anti-arthritic, antioxidant and *in vitro* cytotoxicity activities. *New Journal of Chemistry*, 2017, 41(18): 10347−10356. https://doi.org/10.1039/C7NJ02664A

[2] K.B. Narayanan, N. Sakthivel. Green synthesis of biogenic metal nanoparticles by terrestrial and aquatic phototrophic and heterotrophic eukaryotes and biocompatible agents. *Advances in Colloid and Interface Science*, 2011, 169(2): 59−79. https://doi.org/10.1016/j.cis.2011.08.004

[3] A.A. Ezhilarasi, J.J. Vijaya, K. Kaviyarasu, et al. Green synthesis of nickel oxide nanoparticles using Solanum trilobatum extract for cytotoxicity, antibacterial and photocatalytic studies. *Surfaces and Interfaces*, 2020, 20: 100553. https://doi.org/10.1016/j.surfin.2020.100553

[4] K. Periyasamy, S. Kaliyaperumal, Eco-friendly synthesis of silver nanoparticles using Ventilago maderaspatana (GAERTN), their morphological characterization. *International Journal of ChemTech Research*, 2017, 10 (9): 01–06.

[5] M. Anandan, G. Poorani, P. Boomi, et al. Green synthesis of anisotropic silver nanoparticles from the aqueous leaf extract of *Dodonaea viscosa* with their antibacterial and anticancer activities. *Process Biochemistry*, 2019, 80: 80−88. https://doi.org/10.1016/j.procbio.2019.02.014

[6] Y.-J. Choi, H.-H. Park. Direct patterning of SnO_2 composite films prepared with various contents of Pt nanoparticles by photochemical metal-organic deposition. *Thin Solid Films*, 2011, 519(19): 6214−6218. https://doi.org/10.1016/j.tsf.2011.03.051

[7] C. Dagdeviren, S.W. Hwang, Y. Su, et al. Transient, biocompatible electronics and energy harvesters based on ZnO. *Small*, 2013, 9(20): 3398−3404. https://doi.org/10.1002/smll.201300146

[8] J.W. Rasmussen, E. Martinez, P. Louka, et al. Zinc oxide nanoparticles for selective destruction of tumor cells and potential for drug delivery applications. *Expert Opinion on Drug Delivery*, 2010, 7(9): 1063−1077. https://doi.org/10.1517/17425247.2010.502560

[9] L. Nie, L. Gao, P. Feng, et al. Three-dimensional functionalized tetrapod-like ZnO nanostructures for plasmid DNA delivery. *Small*, 2006, 2(5): 621−625. https://doi.org/10.1002/smll.200500193

[10] G. Applerot, A. Lipovsky, R. Dror, et al. Enhanced antibacterial activity of nanocrystalline ZnO due to increased ROS-mediated cell injury. *Advanced Functional Materials*, 2009, 19(6): 842−852. https://doi.org/10.1002/adfm.200801081

[11] A. Alkaladi, A.M. Abdelazim, M. Afifi. Antidiabetic activity of zinc oxide and silver nanoparticles on streptozotocin-induced diabetic rats. *International Journal of Molecular Sciences*, 2014, 15(2): 2015−2023. https://doi.org/10.3390/ijms15022015

[12] N. Grara, M. Bouloudenine, F. Khaldi, et al. Caractérisation morphophysiologique de la Toxicité du ZnO (Nanoparticule manufacturée) sur l'escargot l' *Helix aspersa* bio indicateur de pollution de l'environnement. *Journal of Materials and Environmental Science*, 2015, 6(9): 2596−2603.

[13] I. Bibi, N. Nazar, M. Iqbal, et al. Green and eco-friendly synthesis of cobalt-oxide nanoparticle: characterization and photo-catalytic activity. *Advanced Powder Technology*, 2017, 28(9): 2035−2043. https://doi.org/10.1016/j.apt.2017.05.008

[14] J. Santhoshkumar, S.V. Kumar, S. Rajeshkumar. Synthesis of zinc oxide nanoparticles using plant leaf extract against urinary tract infection pathogen. *Resource-Efficient Technologies*, 2017, 3(4): 459−465. https://doi.org/10.1016/j.reffit.2017.05.001

[15] J.L. Gardea-Torresdey, E. Gomez, J. Peralta-Videa, et al. Alfalfa sprouts: A natural source for the synthesis of silver nanoparticles. *Langmuir*, 2003, 19(4): 1357−1361. https://doi.org/10.1021/la020835i

[16] V.V. Makarov, A.J. Love, O.V. Sinitsyna, et al. Green nanotechnologies: synthesis of metal nanoparticles using plants. *Acta Naturae*, 2014, 6(1): 35−44. https://doi.org/10.32607/20758251-2014-6-1-35-44

[17] A. Raja, S. Ashokkumar, R. Pavithra Marthandam, et al. Eco-friendly preparation of zinc oxide nanoparticles using *Tabernaemontana divaricata* and its photocatalytic and antimicrobial activity. *Journal of Photochemistry and Photobiology B*: *Biology*, 2018, 181: 53−58. https://doi.org/10.1016/j.jphotobiol.2018.02.011

[18] M.S. Shekhawat, M. Manokari. Biogenesis of zinc oxide nanoparticles using Morinda pubescens J.E, Smith extracts and their characterization. *International Journal of Biomedical Engineering and Technology*, 2014, 5(1): 1−6.

[19] I. Hussain, N.B. Singh, A. Singh, et al. Green synthesis of nanoparticles and its potential application. *Biotechnology Letters*, 2016, 38(4): 545−560. https://doi.org/10.1007/s10529-015-2026-7

[20] Jaishree, Sachin. Natural products and by-products as a cost-effective adsorbent for Cr (VI) removal from water sources: a review. *Austin Environmental Sciences*, 2022, 7(2): 1074. https://doi.org/10.26420/austinenvironsci.2022.1074

[21] M. Naseer, U. Aslam, B. Khalid, et al. Green route to synthesize Zinc Oxide Nanoparticles using leaf extracts of Cassia fistula and *Melia azadarach* and their antibacterial potential. *Scientific Reports*, 2020, 10: 9055. https://doi.org/10.1038/s41598-020-65949-3

[22] Sachin, Jaishree, N. Singh, et al. Green synthesis of Zinc Oxide Nanoparticles using lychee peel and its application in anti-bacterial properties and CR dye removal from wastewater. *Chemosphere*, 2023, 327: 138497. https://doi.org/10.1016/j.chemosphere.2023.138497

[23] A. Aziz, Z. Memon, A. Bhutto. Efficient photocatalytic degradation of industrial wastewater dye by *Grewia asiatica* mediated zinc oxide nanoparticles. *Optik*, 2023, 272: 170352. https://doi.org/10.1016/J.IJLEO.2022.170352

[24] M.A. Abomuti, E.Y. Danish, A. Firoz, et al. Green synthesis of zinc oxide nanoparticles using *Salvia officinalis* leaf extract and their photocatalytic and antifungal activities. *Biology*, 2021, 10(11): 1075. https://doi.org/10.3390/biology10111075

[25] M. MuthuKathija, M.S.M. Badhusha, V. Rama. Green synthesis of zinc oxide nanoparticles using *Pisonia Alba* leaf extract and its antibacterial activity. *Applied Surface Science Advances*, 2023, 15: 100400. https://doi.org/10.1016/j.apsadv.2023.100400

[26] K.M. Ezealisiji, X. Siwe-Noundou, B. Maduelosi, et al. Green synthesis of zinc oxide nanoparticles using *Solanum torvum* (L) leaf extract and evaluation of the toxicological profile of the ZnO nanoparticles–hydrogel composite in Wistar albino rats. *International Nano Letters*, 2019, 9: 99−107. https://doi.org/10.1007/s40089-018-0263-1

[27] U.L. Ifeanyichukwu, O.E. Fayemi, C.N. Ateba. Green synthesis of zinc oxide nanoparticles from pomegranate (*Punica granatum*) extracts and characterization of their antibacterial activity. *Molecules*, 2020, 25: 4521. https://doi.org/10.3390/molecules25194521

[28] E.E. Imade, T.O. Ajiboye, A.E. Fadiji, et al. Green synthesis of zinc oxide nanoparticles using plantain peel extracts and the evaluation of their antibacterial activity. *Scientific African*, 2022, 16: e01152. https://doi.org/10.1016/j.sciaf.2022.e01152

[29] N. Vijayakumar, V.K. Bhuvaneshwari, G.K. Ayyadurai, et al. Green synthesis of zinc oxide nanoparticles using *Anoectochilus elatus*, and their biomedical applications. *Saudi Journal of Biological Sciences*, 2022, 29(4): 2270−2279. https://doi.org/10.1016/j.sjbs.2021.11.065

[30] P.C. Nagajyothi, S.J. Cha, I.J. Yang, et al. Antioxidant and anti-inflammatory activities of zinc oxide nanoparticles synthesized using *Polygala tenuifolia* root extract. *Journal of Photochemistry and Photobiology B*: *Biology*, 2015, 146: 10−17. https://doi.org/10.1016/j.jphotobiol.2015.02.008

[31] N.A. Al-Dhabi, M.V. Arasu. Environmentally-friendly green approach for the production of zinc oxide nanoparticles and their anti-fungal, ovicidal, and larvicidal properties. *Nanomaterials*, 2018, 8(7): 500. https://doi.org/10.3390/nano8070500

[32] Y. Dogan, S. Baslar, H. Aydin, et al. A Study of the soil-plant interactions of *Pistacia lentiscus* L. distributed in the western Anatolian part of Turkey. *Acta Botanica Croatica*, 2003, 62(2): 73−88.

[33] N. Smail-Saadoun. Types stomatiques du genre *Pistacia*: *Pistacia atlantica* Desf. ssp. *Atlantica* et *Pistacia lentiscus*. In: XIII GREMPA Meeting on Almonds and Pistachios. Zaragoza: CIHEAM, 2005: 369–371.

[34] A. Bouyahya, N. Dakka, A. Talbaoui, et al. Phenolic contents and antiradical capacity of vegetable oil from *Pistacia lentiscus* (L). *Journal of Materials and Environmental Science*, 2018, 9: 1518−1524.

[35] H. Benamar, A. Marouf, M. Bennaceur. Phytochemical composition, antioxidant and acetylcholinesterase inhibitory activities of aqueous extract and fractions of *Pistacia atlantica* subsp. *atlantica* from Algeria. *Journal of Herbs*, *Spices* & *Medicinal Plants*, 2018, 24(3): 229−244. https://doi.org/10.1080/10496475.2018.1446204

[36] P. Ribéreau-Gayon. Les composés phénoliques des végétaux. Edition Dunod, Paris, 1968: 254.

[37] R. Paris, H. Moyse. Précis de matière médicinale. Paris: Masson, 1969.

[38] J.B. Harborne. Phytochemical methods. A Guide to Modern Techniques of Plant Analysis, (Third Edition). Netherlands: Springer, 1998: 302.

[39] J. Bruneton. Pharmacognosie, Phytochimie et Plantes Médicinales (3ème Edition). Paris: Médicales Internationales et Tec & Doc, 1999: 1120.

[40] W.C. Evans, E. Trease. Pharmacognosy E-Book. Elsevier Health Sciences, 2009.

[41] V.L. Singleton, R. Orthofer, R.M. Lamuela-Raventós. Analysis of total phenols and other oxidation substrates and antioxidants by means of folin-ciocalteu reagent. *Methods in Enzymology*, 1999: 152–177. https://doi.org/10.1016/S0076-6879(99)99017-1

[42] M. Gaytan-Martínez, A.H. Cabrera-Ramírez, E. Morales-Sanchez et al. Effect of nixtamalization process on the content and composition of phenolic compounds and antioxidant activity of two sorghums varieties. *Journal of Cereal Science*, 2017, 77: 1−8. https://doi.org/10.1016/j.jcs.2017.06.014

[43] I., Kosalec, M. Bakmaz, S. Pepeljnjak, et al. Quantitative analysis of the flavonoids in raw propolis from northern Croatia. *Acta Pharmaceutica*, 2004, 54(1): 65−72.

[44] R.B. Broadhurst, W.T. Jones. Analysis of condensed tannins using acidified vanillin. *Journal of the Science of Food and Agriculture*, 1978, 29(9): 788−794. https://doi.org/10.1002/jsfa.2740290908

[45] F.T. Thema, E. Manikandan, M.S. Dhlamini, et al. Green synthesis of ZnO Nanoparticles via *Agathosma betulina* natural extract. *Materials Letters*, 2015, 161: 124−127. https://doi.org/10.1016/j.matlet.2015.08.052

[46] T.U. Doan Thi, T.T. Nguyen, Y.D. Thi, et al. Green synthesis of ZnO nanoparticles using orange fruit peel extract for antibacterial activities. *RSC Advances*, 2020, 10: 23899−23907. https://doi.org/10.1039/d0ra04926c

[47] H. Huang, and X. Yang. Synthesis of polysaccharide-stabilized gold and silver nanoparticles: A green method.

Carbohydrate Research, 2004, 339(15): 2627−2631. https://doi.org/10.1016/j.carres.2004.08.005

[48] M.M.R. Mollick, D. Rana, S.K. Dash, et al. Studies on green synthesized silver nanoparticles using *Abelmoschus esculentus* (L.) pulp extract having anticancer (*in vitro*) and antimicrobial applications. *Arabian Journal of Chemistry*, 2019, 12(8): 2572−2584. https://doi.org/10.1016/j.arabjc.2015.04.033

[49] Y. Shin, I-T. Bae, B.W. Arey, et al. Facile stabilization of gold-silver alloy nanoparticles on cellulose nanocrystal. *The Journal of Physical Chemistry C*, 2008, 112(13): 4844−4848. https://doi.org/10.1021/jp710767w

[50] C. Fong, D. Wells, I. Krodkiewska, et al. New role for urea as a surfactant headgroup promoting self-assembly in water. *Chemistry of Materials*, 2006, 18: 594. https://doi.org/10.1021/cm0522681

[51] M.S. Blois. Antioxidant determinations by the use of a stable free radical. *Nature*, 1958, 181: 1199−1200. https://doi.org/10.1038/1811199a0

[52] R. Subramanian, P. Subbramaniyan, V. Raj. Double bypasses soxhlet apparatus for extraction of piperine from *Piper nigrum*. *Arabian Journal of Chemistry*. 2011, 9: S537–S540. https://doi.org/10.1016/j.arabjc.2011.06.022

[53] R. M.Samarth, M. Panwar, A. Soni et al., Evaluation of antioxidant and radical scavenging activities of certain radioprotective plant extract. *Food Chemistry*, 2008, 106: 868–873. https://doi.org/10.1016/j.foodchem.2007.05.005

[54] S nchez-Moreno, C., Larrauri, J. A., Saura-Calixto, F. A procedure to measure the antiradical efficiency of polyphenols. *Journal of the Science of Food and Agriculture*, 1998, 76(2): 270276. https://doi.org/10.1002/(SICI)1097-0010(199802)76:2<270::AID-JSFA945>3.0.CO;2-9

[55] Y.M. Choi, D.O. Noh, S.Y. Cho et al. Antioxidant and antimicrobial activities of propolis from several regions of Korea. *Lebensmittel-Wissenschaft & Technologie LWT*, 2006, 39: 756−761. https://doi.org/10.1016/j.lwt.2005.05.015

[56] A.G. Ponce, R. Fritz, C. del Valle, et al. Antimicrobial activity of essential oils on the native microflora of organic Swiss chard. *LWT - Food Science and Technology*, 2003, 36(7): 679−684. https://doi.org/10.1016/S0023-6438(03)00088-4

[57] Clinical and Laboratory Standards Institute. Performance Standards for Antimicrobial Disk Susceptibility Tests; Approved Standard-Tenth Edition M02-A10. 2009.

[58] M.J. Rodríguez Vaquero, M.R. Alberto, M.C. Manca de Nadra. Influence of phenolic compounds from wines on the growth of *Listeria monocytogenes*. *Food Control*, 2007, 18(5): 587–593. https://doi.org/10.1016/j.foodcont.2006.02.005

[59] F. Konan Kouadio, N.K. Guessennd, O. Karamoko, et al. Action antibactérienne de l'extrait éthanolique 70% de *Clerodendrum splendens* (G. Don) (Verbenacae) sur des souches bactériennes isolées de selles chez des enfants diarrhéiques. *International Journal of Biological and Chemical Sciences*, 2013, 7(3): 1332−1337. https://doi.org/10.4314/ijbcs.v7i3.38

[60] A.A. Mamonier. Introduction aux techniques d'étude des antibiotiques. In: Bactériologie Médicale, Technique Usuelles. Doin: Paris, 1990: 227–236.

[61] M. Barbouchi, K. Elamrani, M. El Idrissi, et al. A comparative study on phytochemical screening, quantification of phenolic contentsand antioxidant properties of different solvent extracts from various parts of *Pistacia lentiscus* L. *Journal of King Saud University – Science*, 2018, 32(1): 12. https://doi.org/10.1016/j.jksus.2018.05.010

[62] A. Maalej, W. Elloumi, I. Angelov, et al. *Pistacia lentiscus* by-product as a promising source of phenolic compounds and carotenoids: Purification, biological potential and binding properties. *Food and Bioproducts Processing*, 2021, 126: 245–255. https://doi.org/10.1016/j.fbp.2021.01.011

[63] A. Cherbal, M. Kebieche, K. Madani, et al. Extraction and valorization of phenolic compounds of leaves of Algerian *Pistacia lentiscus*. *Asian Journal of Plant Sciences*, 2012, 11(3): 131–136. https://doi.org/10.3923/ajps.2012.131.136

[64] S. Remila, D. Atmani-Kilani, S. Delemasure, et al. Antioxidant, cytoprotective, anti-inflammatory and anticancer activities of *Pistacia lentiscus* (Anacardiaceae) leaf and fruit extracts. *European Journal of Integrative Medicine*, 2015, 7(3): 274−286. https://doi.org/10.1016/j.eujim.2015.03.009

[65] H. Bouriche, A. Saidi, A. Ferradji, et al. Anti-inflammatory and immunomodulatory properties of *Pistatia lentiscus* extracts. *Journal of Applied Pharmaceutical Science*, 2016, 6(7): 140−146. https://doi.org/10.7324/JAPS.2016.60721

[66] A. Bampouli, K. Kyriakopoulou, G. Papaefstathiou, et al. Evaluation of total antioxidant potential of Pistacia lentiscus var. chia leaves extracts using UHPLC–HRMS. *Journal of Food Engineering*, 2015, 167: 25−31. https://doi.org/10.1016/j.jfoodeng.2014.10.021

[67] S. Bakli, D. Harzallah, A. Zerroug, et al. Antimicrobial and antioxidant activities of flavonoids extracted from *Pistacia lentiscus* L., leaves. *Journal of Drug Delivery & Therapeutics*, 2020, 10(1-s): 83−89. https://doi.org/10.22270/jddt.v10i1-s.3895

[68] M. Cheurfa, R. Allem, Study of hypocholesterolemic activity of Algerian *Pistacia lentiscus* leaves extracts *in vivo*. *Revista Brasileira de Farmacognosia*, 2015, 25(2): 142–144. https://doi.org/10.1016/j.bjp.2015.02.011

[69] J.-J. Macheix, A. Fleuriet, C. Jay-Allemand. Les Composés Phénoliques des Végétaux. Lausanne: Presses Polytechniques et Universitaires Romandes éd., 2005: 192.

[70] D. Atmani, N. Chaher, M. Berboucha, et al. Antioxidant capacity and phenol content of selected Algerian medicinal plants. *Food Chemistry*, 2009, 112(2): 303−309. https://doi.org/10.1016/j.foodchem.2008.05.077

[71] G.T. Anand, D. Renuka, R. Ramesh, et al. Green synthesis of ZnO nanoparticle using *Prunus dulcis* (almond gum) for antimicrobial and supercapacitor applications. *Surfaces and Interfaces*, 2019, 17: 100376. https://doi.org/10.1016/j.surfin.2019.100376

[72] J. Osuntokun, C. Damian, E. Onwudiwe, et al. Green synthesis of ZnO nanoparticles using aqueous *Brassica oleracea* L. var. *italica* and the photocatalytic activity. *Green Chemistry Letters and Reviews*, 2019, 12(4): 444−457. https://doi.org/10.1080/17518253.2019.1687761

[73] A.J. Rush Jr., M.B. First, D. Blacker. Handbook of Psychiatric Measures. American Psychiatric Publishing, Inc, 2008: 86.

[74] R.M. Silverstein, F.X. Webster, D.J. Kiemle, et al. Spectrometric Identification of Organic Compounds. John wiley and sons, 2014: 86.

[75] R. Myriam. Aide au repérage des Nanomatériaux en Entreprise. INRS, 2014: 17–35.

[76] A.C. Taş, P.J. Majewski, F. Aldinger. Chemical preparation of pure and strontium- and/or magnesium - doped lanthanum gallate powders. *Journal of the American Ceramic Society*, 2000, 83(12): 2954−2960. https://doi.org/10.1111/j.1151-2916.2000.tb01666.x

[77] R. Kumar, G. Kumar, A. Umar. ZnO nano-mushrooms for photocatalytic degradation of methyl orange. *Materials Letters*, 2013, 97: 100−103. https://doi.org/10.1016/j.matlet.2013.01.044

[78] A.B. Lavand, Y.S. Malghe. Visible light photocatalytic degradation of 4-chlorophenol using C/ZnO/CdS nanocomposite. *Journal of Saudi Chemical Society*, 2015, 19: 471−478. https://doi.org/10.1016/j.jscs.2015.07.001

[79] M. Jabeena, M.A. Iqbala, R.V. Kumarb, et al. Chemical synthesis of zinc oxide nanorods forenhanced hydrogen gas sensing. *Chinese Physics* B, 2014, 23(1): 018504. https://doi.org/10.1088/1674-1056/23/1/018504

[80] P. Scherrer. Bestimmung der inneren Struktur und der Größe von Kolloidteilchen mittels Röntgenstrahlen. In: Kolloidchemie Ein Lehrbuch. Berlin, Heidelberg: Springer, 1912: 387–409. https://doi.org/10.1007/978-3-662-33915-2_7

[81] D. Belhachat, F. Aid, L. Mekimene, et al. Phytochemical screening and *in vitro* antioxidant activity of *Pistacia lentiscus* berries ethanolic extract growing in Algeria. *Mediterranean Journal of Nutrition and Metabolism*, 2017, 10: 273−285. https://doi.org/10.3233/MNM-17169

[82] R. Hemma, S. Belhadj, C. Ouahchia, et al. Antioxidant activity of *Pistacia lentiscus* methanolic extracts. *Revue Agrobiologia*, 2018, 8(1): 845−852.

[83] A.I. Ghenima, M. Idir, M.G. Nadjet, et al. *In vitro* evaluation of biological activities of *Pistacia lentiscus* aqueous extract. *International Journal of Pharmacy and Pharmaceutical Sciences*, 2015, 7(11): 133–139.

[84] K.E. Heim, A.R. Tagliaferro, D.J. Bobilya. Flavonoid antioxidants: chemistry, metabolism and structure-activity relationships. *Journal of Nutritional Biochemistry*, 2002, 13(10): 572−584. https://doi.org/10.1016/S0955-2863(02)00208-5

[85] N.T. Erol, F. Sarı, Y.S. Velioglu. Polyphenols, alkaloids and antioxidant activity of different grades Turkish black tea. *GIDA*, 2010, 35(3): 161−168.

[86] A.d.P. Bidie, B.B. N'Guessan, A.F. Yapo, et al. Activités antioxydantes de dix plantes medicinales de la pharmacopée ivoirienne. *Sciences & Nature*, 2011, 8(1): 1−11.

[87] T. Andzi Barhé, G.R. Feuya Tchouya. Comparative study of the anti-oxidant activity of the total polyphenols extracted from *Hibiscus sabdariffa* L., *Glycine max* L. *Merr.*, yellow tea and red wine through reaction with DPPH free radicals. *Arabian Journal of Chemistry*, 2016, 9(1): 1−8. https://doi.org/10.1016/j.arabjc.2014.11.048

[88] S. Roy, J.-W. Rhim. Carrageenan-based antimicrobial bionanocomposite films incorporated with ZnO nanoparticles stabilized by melanin. *Food Hydrocolloids*, 2019, 90: 500−507. https://doi.org/10.1016/j.foodhyd.2018.12.056

[89] J.J. Fleurette, M. Freney, E. Reverdy. Antiseptie et désinfection. Paris: ESKA Editions, 1995.

[90] M.S. Ali-Shtayeh, R.M.-R. Yaghmour, Y.R. Faidi, et al. Antimicrobial activity of 20 plants used in folkloric medicine in the Palestinian area. *Journal of Ethno Pharmacology*, 1998, 60: 265−271. https://doi.org/10.1016/s0378-8741(97)00153-0

[91] G. Sharmila, C. Muthukumaran, K. Sandiya, et al. Biosynthesis, characterization, and antibacterial activity of zinc oxide nanoparticles derived from *Bauhinia tomentosa* leaf extract. *Journal of Nanostructure in Chemistry*, 2018, 8: 293−299. https://doi.org/10.1007/s40097-018-0271-8

[92] M. Iswarya, P. Sudha, V. Kalaiselvi, et al. Solanum nigrum leaf extract capped synthesis of ZnO nanoparticles. *Journal of Environmental Nanotechnology*, 2020, 9: 37−41. https://doi.org/10.13074/jent.2020.12.204424

[93] J. Vidic, S. Stankic, F. Haque, et al. Selective antibacterial effects of mixed ZnMgO nanoparticles. *Journal of Nanoparticle Research*, 2013, 15(5): 1595. https://doi.org/10.1007/s11051-013-1595-4

[94] N.H. Aysa, H.D. Salman. Antibacterial activity of modified zinc oxide nanoparticles against Pseudomonas aeruginosa isolates of burn infections. *World Scientific News*, 2016, 33: 1−14.

[95] U. Kadiyala, E.S. Turali-Emre, J.H. Bahng, et al. Unexpected insights into antibacterial activity of zinc oxide nanoparticles against methicillin resistant *Staphylococcus aureus* (MRSA). *Nanoscale*, 2018, 10: 4927−4939. https://doi.org/10.1039/C7NR08499D

[96] H. Zhang, G. Chen. Potent antibacterial activities of Ag/TiO2 nanocomposite: powders synthesized by a one-pot sol−gel method. *Environmental Science & Technology*, 2009, 43(8): 2905−2910. https://doi.org/10.1021/es803450f

[97] K. Kairyt, A. Kadys, Z. Luksiene. Antibacterial and antifungal activity of photo activated ZnO nanoparticles in suspension. *Journal of Photochemistry and Photobiology B*: *Biology*, 2013, 128: 78−84. https://doi.org/10.1016/j.jphotobiol.2013.07.017

[98] A. Sirelkhatim, S. Mahmud, A. Seeni, et al. Review on zinc oxide nanoparticles: Antibacterial activity and toxicity mechanism. *Nano Micro Letters*, 2015, 7: 219−242. https://doi.org/10.1007/s40820-015-0040-x

[99] Y.-W. Huang, C.-H. Wu, R.S. Aronstam. Toxicity of transition metal oxide nanoparticles: Recent insights from *in vitro* studies. *Materials*, 2010, 3(10): 4842−4859. https://doi.org/10.3390/ma3104842

[100] Z.B. Huang, X. Zheng, D.H. Yan, et al. Toxicological effect of ZnO nanoparticles based on bacteria. *Langmuir*, 2008, 24(8): 4140−4144. https://doi.org/10.1021/la7035949

[101] M.J. Hajipour, K.M. Fromm, A.A. Ashkarran, et al. Antibacterial properties of nanoparticles. *Trends in Biotechnology*, 2012, 30(10): 499−511. https://doi.org/10.1016/j.tibtech.2012.06.004

[102] A. Kumar, A.K. Pandey, S.S. Singh et al. Engineered ZnO and TiO_2 nanoparticles induce oxidative stress and DNA damage leading to reduced viability of *Escherichia coli*. *Free Radical Biology and Medicine*, 2011, 51: 1872−1881. https://doi.org/10.1016/j.freeradbiomed.2011.08.025

[103] Z. Xia, J. Min, S. Zhou, et al. Photocatalytic performance and antibacterial mechanism of Cu/Ag-molybdate powder material. *Ceramics International*, 2021, 47(9): 12667−12679. https://doi.org/10.1016/j.ceramint.2021.01.127

[104] Y. Liu, L. He, A. Mustapha, et al. Antibacterial activities of zinc oxide nanoparticles against *Escherichia coli* O157:H7. *Journal of Applied Microbiology*, 2009, 107(4): 1193−1201. https://doi.org/10.1111/j.1365-2672.2009.04303.x